Journal of Solid State Chemistry 184 (2011) 488–493

Contents lists available at ScienceDirect

Journal of Solid State Chemistry

journal homepage: www.elsevier.com/locate/jssc

Silylated Co/SBA-15 catalysts for Fischer–Tropsch synthesis

Lihong Jia [a,b], Litao Jia [a], Debao Li [a,*], Bo Hou [a], Jungang Wang [a,b], Yuhan Sun [a,*]

[a] State Key Laboratory of Coal Conversion, Institute of Coal Chemistry, The Chinese Academy of Sciences, Taiyuan 030001, Shanxi, China
[b] Graduate University of Chinese Academy of Sciences, Beijing 100049, China

ARTICLE INFO

Article history:
Received 29 June 2010
Received in revised form
18 September 2010
Accepted 3 October 2010
Available online 5 November 2010

Keywords:
Vapor-phase silylation
Cobalt
SBA-15
Fischer–Tropsch synthesis

ABSTRACT

A series of silylated Co/SBA-15 catalysts were prepared via the reaction of surface Si–OH of SBA-15 with hexamethyldisilazane (HMDS) under anhydrous, vapor-phase conditions, and then characterized by FT-IR, N_2 physisorption, TG, XRD, and TPR-MS. The results showed that organic modification led to a silylated SBA-15 surface composed of stable hydrophobic Si–$(CH_3)_3$ species even after calcinations and H_2 reduction at 673 K. Furthermore, the hydrophobic surface strongly influenced both metal dispersion and reducibility. Compared with non-silylated Co/SBA, Co/S-SBA (impregnation after silylation) showed a high activity, due to the better cobalt reducibility on the hydrophobic support. However, S-Co/SBA (silylation after impregnation) had the lowest FT activity among all the catalysts, due to the lower cobalt reducibility along with the steric hindrance of grafted –Si$(CH_3)_3$ for the re-adsorption of α-olefins.

1. Introduction

Since the Mobil Oil Corporation discovered the M41s group of mesoporous materials in 1992, preparation of inorganic–organic hybrid materials by introducing functional organic groups to the pore surface of the mesoporous silica materials has attracted considerable attention [1,2], which was due to the potential applications of the resultant materials in the field of catalysis [3,4], separation [5], adsorption of heavy metals [6], chemical sensing [7], and nanoscience [8,9]. Owing to the potential advantage of changing the surface physical and chemical properties of mesoporous silicates, the silylation technique has received much research interest in the field of catalysis [10]. Generally, two approaches were developed for the surface functionalization, including direct co-condensation synthesis [11] and post-synthesis grafting [12]. The co-condensation synthesis would be the first choice for a higher and more uniform surface coverage with functional groups [13]. It also provided a better control over the amount of organic groups incorporated in the resultant materials. However, the structural order of the host materials would be destroyed in the direct synthesis method. In contrast with the co-condensation method, post-synthesis grafting silylation was of simplicity and versatility, given the wide variety of commercially available silylation agents. Furthermore, the products obtained by post-grafting method were often better defined structurally and more stable hydrolytically.

Fischer–Tropsch (FT) synthesis is an important catalytic process which was well-known to produce ultraclean alternative fuels from coal, natural gas and biomass via syngas [14]. Cobalt-based catalysts have been widely applied in an FT synthesis owing to their high activity, high selectivity towards long chain *n*-paraffins, and their lower activity for the competing water gas shift reaction (WGSR) [15]. The FT synthesis activity over cobalt catalyst depended primarily on the overall amount of an exposed metallic cobalt during the reduction process, which was determined by the cobalt loading amount, metal particle size, dispersions and reduction degree [16,17]. Furthermore, the chemical and texture properties of the support influenced the catalytic activity and product selectivity of cobalt catalysts via their modifications on the reducibility and dispersion of cobalt or the formation of well-fined phases. Sometimes it might be more economical to modify or change the support properties than to increase the number of active sites.

It has been shown that the control of hydrophilic/hydrophobic properties of supports were of importance in the preparation of catalysts and in determining the catalytic behavior [18,19]. Especially, an FT synthesis is the hydrothermal reaction, because the amount of water is produced along with the main reaction. Several researchers reported the impact of support hydrophobicity on the catalyst activity in the Fischer–Tropsch synthesis. For example, Kim et al. [20] showed that the preliminary silylation of an SBA-15 support enhanced the reducibility of the cobalt oxide species due to the weaker cobalt oxide-support interaction and consequently promoted the activity for the FT synthesis. Ojeda et al. [21] reported that the CO conversion rate increased over the silylated catalyst, because the hydrophobic surface expelled the water molecules and more surface sites were available for CO adsorption and dissociation. In our previous study, Shi et al. [22] found that

* Corresponding authors. Fax: +86 351 4041153.
E-mail addresses: dbli@sxicc.ac.cn (D. Li), yhsun@sxicc.ac.cn (Y. Sun).

0022-4596/$ - see front matter © 2010 Elsevier Inc. All rights reserved.
doi:10.1016/j.jssc.2010.10.002

CH_3-modified Co/Ru/SiO_2 catalysts showed a higher selectivity towards C_5–C_{11} hydrocarbons, which should be ascribed to its hydrophobic characteristics. However, all the modification processes were carried out in the liquid phase reaction, which required the use and disposal of nonaqueous solvents. Vapor-phase silylation offers several advantages over the liquid-phase silylation: (i) mass transport rates are generally higher in the vapor phase, and hence silylation reaction rates; (ii) vapor-phase silylation reaction conditions can also be more easily controlled, resulting in more reproducible surface modifications; and (iii) vapor-phase silylation methods are more cost-effective and environmentally friendly than liquid-phase procedures. However, few literatures were reported using such a silylation method during the preparation of cobalt-supported catalysts. Here, the vapor-phase silylation was employed in the preparation of mesoporous cobalt catalysts. Co/SBA-15 was silylated by different post-grafting synthesis routes under anhydrous, vapor-phase reaction conditions. Both silylated and non-silylated catalysts were tested for the F–T synthesis to understand the effect of silylation procedure on the activity and selectivity.

2. Experimental

2.1. Samples preparation

1,1,1,3,3,3-Hexamethyldisilazane (HMDS) (Alfa Aesar, $>99.9\%$, CAS no. 999-97-3) was used as the silylant reagent. The procedure employed for the silylation of the samples was as follows: a sample of an SBA-15 (purchased from the Fudan University) was previously evacuated at 423 K for 3 h to remove any residual surface water and then cooled down to room temperature in vacuum and transferred into a 500 ml beaker. The HMDS in another 1000 ml beaker was boiled at 333 K and the resulting gas was reacted with SBA-15 for two days in water bath at 333 K. After treating with HDMS, the modified supports were dried at 328 K in vacuum overnight to remove adsorbed NH_3 and unreacted silylating agent. The corresponding reaction scheme was as follows:

$$Si{-}OH + (CH_3)_3Si{-}NH{-}Si\,(CH_3)_3 \rightarrow Si{-}O{-}Si(CH_3)_3 + NH_3\uparrow.$$

The prepared materials would be referred as SBA (non-silylated SBA-15) and S-SBA (silylated SBA-15).

However, an SBA-15-supported Co catalysts with 20 wt% metal loading were prepared by an incipient wetness impregnation of SBA and S-SBA with the required volume of ethanol cobalt nitrate solutions. Then, the cobalt impregnated samples were dried at 393 K and calcined in air at 673 K for 6 h. These catalysts would be denoted as Co/SBA and Co/S-SBA.

Another catalyst S-Co/SBA was prepared under identical conditions, but different route by silylation of the Co/SBA solid. Firstly, cobalt was deposited over the bare SBA-15 support, and then the obtained material was silylated with HMDS following the silylation procedure described above for an SBA-15.

2.2. Catalyst characterization

FT-IR experiments were perfomed in a Nicolet Magna 550 spectrophotometer using a resolution of 4 cm^{-1} at room temperature. Typically, about 1–5 mg of the sample were diluted by KBr (ratio 1:300) and pressed into a wafer.

The content of carbon, hydrogen and nitrogen was measured with Vario EL Analyzer.

TGA was carried out on a Setaram TGA-92 analyzer with a heating speed of 10 K/min in the 303–1073 K range under air in a flow of 50 ml/min.

Nitrogen adsorption–desorption was performed at 77 K with an ASAP-2000 Micromeritics instrument to obtain BET specific surface areas and BJH pore size distributions. Before the analysis, the samples were outgassed at 393 K for 12 h.

XRD patterns of the samples were collected on a Rigaku D/max-RA instrument with Cu-$K\alpha$ radiation. Small-angle X-ray diffraction data were collected from 0.5° to 5° (2θ) with a resolution of 0.02°. The wide-angle XRD spectra were scanned at a rate of 2.0°/min in the range $2\theta = 20$–80°. The crystallite phase was estimated with the data of JCPDS. The mean Co_3O_4 crystallite sizes were obtained according to the (3 1 1) diffraction peak by the Scherrer equation.

H_2-TPR was performed in a U-tube quartz microreactor heated by an electrical furnace. The reactor was loaded with 25 mg calcined catalyst and heated at a temperature ramp at 10 K/min from 333 to 1233 K with a gas consisting of 5% H_2 in an N_2. The gas flow rate was 60 ml/min. The H_2 consumption (TCD signal) was recorded automatically by a quadrupole mass spectrometer.

2.3. Catalyst testing

All catalysts were evaluated in a stainless-steel fixed-bed reactor at 2.0 MPa, 1000 h^{-1} and a H_2/CO ratio of 2.0. The catalyst loading is 2.0 ml. The catalysts were reduced in a flow of hydrogen at 673 K for 6 h and then cooled down to ambient before switching to syngas. Data were taken at steady state after 24 h on-stream. The gas effluents were analyzed on-line by using a GC-8A chromatographs equipped with thermal conductivity detector (TCD) and flame ionization detectors (FID). Liquid products and wax were collected in a cold trap and a hot trap, respectively, and then were off-line analyzed on a GC-920 chromatograph, which was equipped with a 35 m OV-101 capillary column. The carbon and mass balances were $100 \pm 5\%$.

3. Results and discussion

3.1. Surface grafting

Fig. 1 illustrates the FT-IR spectra of the parent SBA-15 and silylated Co/SBA-15 before and after reduction. As shown in Fig. 1a, for all the samples, the bands at 1083, 806 and 465 cm^{-1} could be assigned to the asymmetric, symmetric stretching and deformation vibrations of the Si–O–Si framework [23,24], respectively. The absorbance at 960 cm^{-1}, corresponding to the Si–O stretching of the Si–OH [25], decreased in the silylated materials as the result of the transformation of Si–OH groups into Si–O–Si$(CH_3)_3$. The broad adsorption at 3470 cm^{-1} was ascribed to free Si–OH groups [26] and another very sharp peak around 1640 cm^{-1} came from physically adsorbed water [27]. Furthermore, the peaks appeared at 2960, 2910 and 1385 cm^{-1}, which were ascribed to C–H stretching and deformation vibrational modes of surface Si–CH_3 formed during the silylation process [28]. These indicated that the surface of an SBA-15 was grafted with methyl groups.

The IR spectra (4000–400 cm^{-1} region) of S-Co/SBA and Co/S-SBA samples were obtained after reduction at 673 K and passivatation. It could be observed that S-Co/SBA sample presented two weak IR bands at 2938 and 2910 cm^{-1} (Fig. 1b), which were ascribed to the symmetric and asymmetric stretching vibrational modes of C–H bonds of the surface Si–CH_3 groups. However, the corresponding methyl groups peaks nearly disppeared for Co/S-SBA, which could be attributed to Si–$(CH_3)_3$ of Co/S-SBA was probably destroyed during the calcination and reduction process at 673 K.

3.2. Thermal stability of silylated catalysts

The thermal stability of silylated samples was investigated by means of thermogravimetric analysis (TGA) techniques (see Fig. 2). The first loss took place at 323–423 K was due to the elimination of

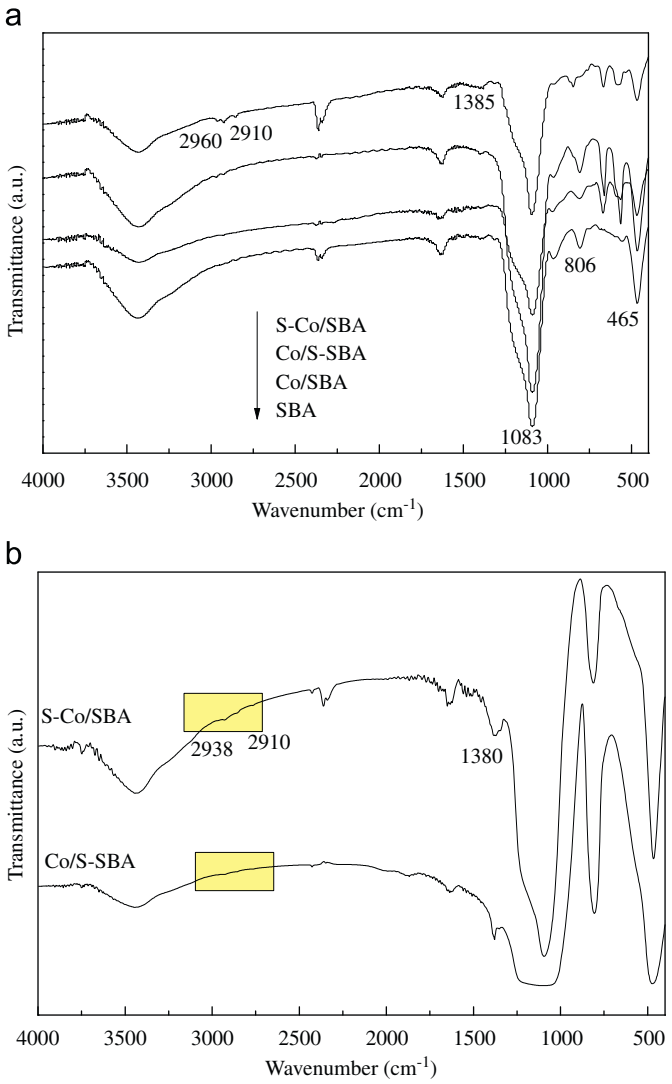

Fig. 1. FT-IR spectra of SBA-15 and surface silylated cobalt catalysts: (a) before reduction process and (b) after reduction process.

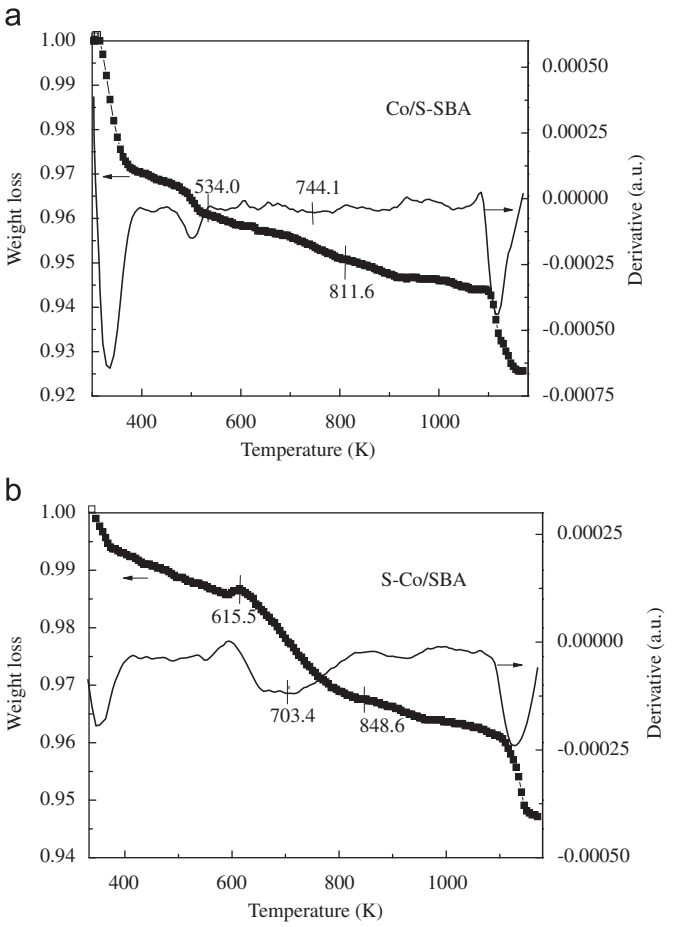

Fig. 2. TG-DTG profiles for the silylated catalysts.

physisorbed water (2–4 wt%). It was well accepted that the amount of desorbed water depended on the surface hydrophobicity [29]. Despite the same amount of HMDS used in the preparation of hydrophobic catalysts, it could be clearly observed that the amount of water desorbed was significantly lower for S-Co/SBA, due to its more hydrophobic surface than Co/S-SBA. The Si–$(CH_3)_3$ species on the surface of Co/S-SBA sample could be partially destroyed during the calcinations at 673 K for 6 h after the impregnation as shown in Table 1. Only a small amount of physisorbed water desorption was detected for the S-Co/SBA. A slight continuous weight loss (1–2 wt%) was observed at 423–873 K, probably associated with the thermal decomposition of methyl groups incorporated in SBA-15. The weight losses above 873 K were likely due to the dehydration of silanol groups on the support surface [30]. Thus, the silylated samples were stable during the calcinations and reduction process at temperatures 673 K. The TGA results were in agreement with the previous infrared spectroscopy results. IR spectroscopy proved that the surface Si-CH_3 groups were stable at temperatures lower than 673 K.

3.3. Phase structure

Fig. 3 shows the X-ray diffractograms of all the silylated SBA-15 catalysts with non-silylated SBA-15 as reference. Silylated SBA-15 catalysts have similar XRD patterns to the pure SBA-15, indicating their ordered hexagonal mesoporous structure (see Fig. 3a). However, the decrease in diffraction intensity and the absence of (1 1 0) and (2 0 0) reflections revealed that their structural order did not remain over a long range, which was usually observed during modification of mesoporous materials [31]. Furthermore, the samples containing cobalt had reflections at 2θ of about 31.3°, 36.9°, 45.0°, 59.4° and 65.2° (see Fig. 3b), corresponding to the different crystal planes of the spinel-phase Co_3O_4 [32]. No other crystalline phase was detected on those catalysts. The particle sizes of Co_3O_4 estimated by the Scherrer equation [33] were listed in Table 1. As expected, the Co_3O_4 crystallite size was slightly larger for Co/S-SBA, due to the weaker cobalt oxide-support interaction. A similar increase in Co_3O_4 crystallite size over a silylated SBA-15 surface was also reported [20]. However, the result of S-Co/SBA disagreed with the results reported by Shi et al. [22], who observed that the silylation did not change the cobalt particle sizes.

3.4. Sample porosity

The isotherms of nitrogen adsorption and desorption for SBA-15, silylated SBA-15 and the corresponding catalysts were illustrated in Fig. 4. The pure-silica SBA-15 sample exhibited a type IV isotherm according to IUPAC with a H1 hysteresis loop, which is characteristic of highly ordered mesoporous materials. For all the silylated SBA-15 and silylated Co/SBA-15 catalysts, the N_2 adsorption isotherms were similar to that of the original SBA-15. These indicated that the parent mesoporous structure was maintained after silylation and cobalt loading, which was in good agreement with the small-angle XRD result.

Table 1
Physical and chemical properties of the support material and the cobalt-SBA-15 catalysts.

Sample	S_{BET} (m^2/g)	V_{Pore} (cm^3/g)	Pore size (nm)	C (wt%)	Co_3O_4 size (nm)[a]	Reducibility (%)[b]
SBA	552	0.94	6.8	–	–	–
S-SBA	407	0.73	7.1	–	–	–
Co/SBA	381	0.60	6.3	0.33	14.3	68.3
Co/S-SBA	338	0.53	6.3	1.29	16.4	71.4
S-Co/SBA	276	0.50	7.3	4.22	15.9	35.8

[a] Calculated from Scherrer equation [33] according to the (3 1 1) diffraction peak of Co_3O_4.
[b] Calculated from the differential area of H_2O during TPR at 333–673 K.

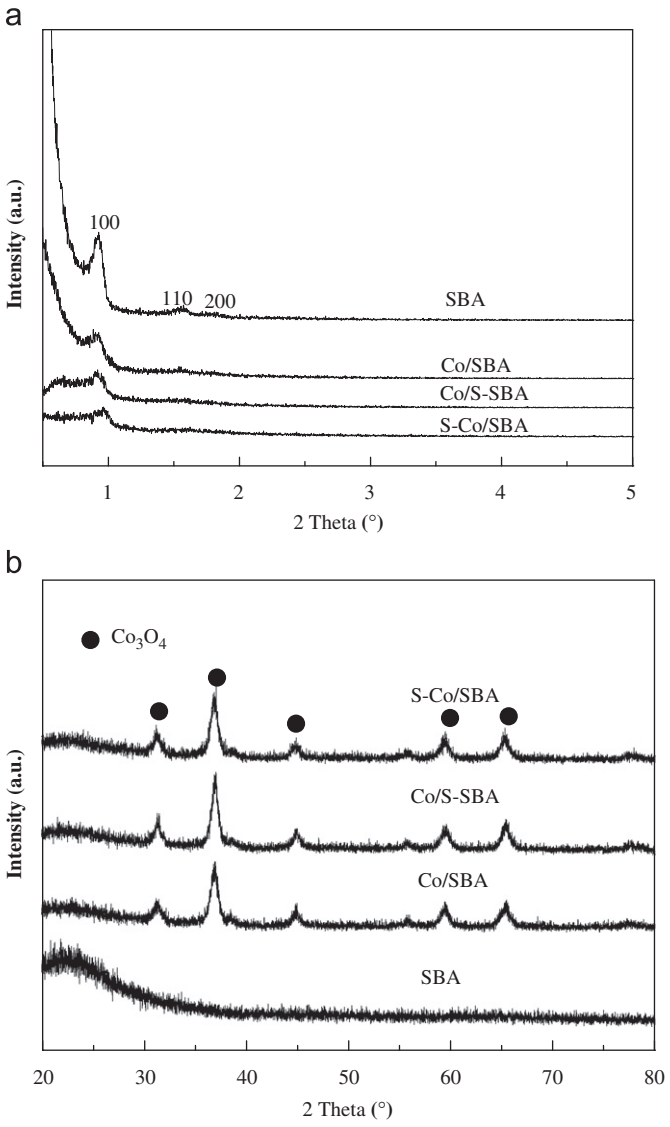

Fig. 3. XRD of the silylated and non-silylated SBA-15 samples.

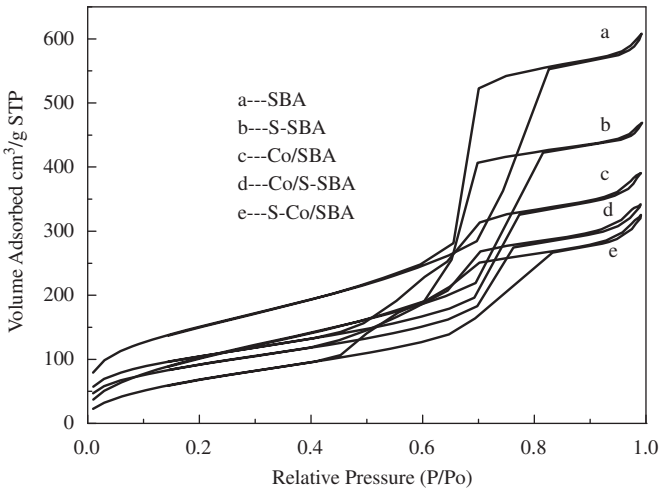

Fig. 4. N_2 adsorption–desorption isotherms of SBA-15, silylated SBA-15 and catalysts.

The BET surface area pore volume and average pore diameter were given in Table 1. Silylation of SBA-15 with HMDS produced a decrease both in specific surface area and in total pore volume, and enlarged the pore size. These could be attributed to the entrance of organic groups into the pores of the support that made them inaccessible for nitrogen adsorption. Meanwhile, organic groups grafted onto the microporous also reduced the surface area and enlarged the average pore diameter.[22] The BET surface area and pore volume decreased further after cobalt impregnation. Impregnation of silicas with cobalt nitrate leads to a pronounced decrease in support concentration in modified catalysts, a "dilution effect," which could also contribute to decrease in catalyst surface areas and pore volume. The pore size of Co/SBA and Co/S-SBA catalysts as smaller than 6.8 nm. This might be caused by a partial blockage of the Co/SBA pores and/or a partial collapse of the mesoporous structure after the silylation with HMDS and cobalt introduction. It was noteworthy that average pore diameter of the catalyst Co/SBA enlarged after silylation, which was primarily attributed to clogging support pores by organic species.

3.5. Reduction behavior

The influence of silylation on the reduction behavior of the Co/SBA catalysts was investigated by TPR, and Fig. 5 shows the H_2-TPR profiles in the temperature range 333–1073 K and the relevant reduction product H_2O ($M/Z=18$) mass analyses. According to the peak of production H_2O, the recorded curves could be divided into three main reduction regions. The first reduction stage at 493–583 K could be assigned to the reduction of Co_3O_4 to CoO, and the second peak at 583–823 K was attributed to the subsequent reduction of intermediate CoO to Co^0 [34]. Besides these two peaks, a broad reduction feature at temperature larger than 823 K could be ascribed to the reduction of cobalt strongly interacted with the support, since bulk Co_3O_4 would be reduced completely at temperature below 773 K [32]. In general, the high temperature reduction peak above 823 K was attributed to the reduction of Co_2SiO_4 [35], although no Co_2SiO_4 phase was observed in an XRD measurement in the present work. Those catalysts appeared the reduction of Co_2SiO_4, except Co/S-SBA. For Co/S-SBA, the silylation before the impregnation might hinder the strong interaction between cobalt precursor and the SBA-15 surface.

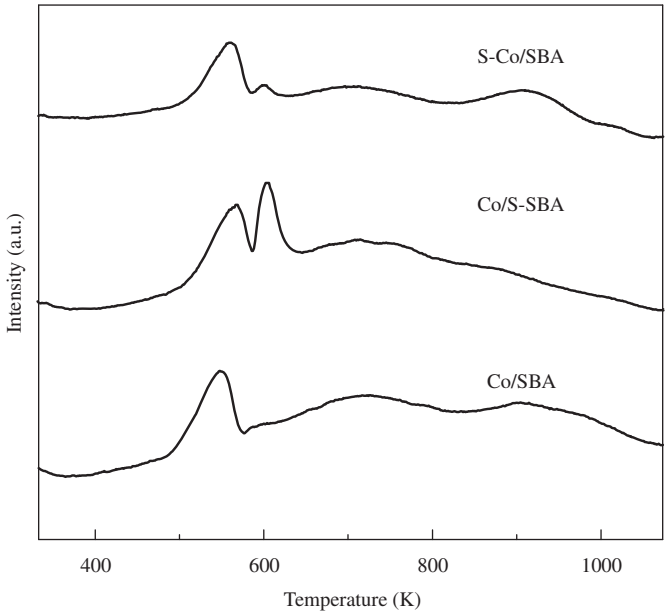

Fig. 5. H_2-TPR-MS profiles of the silylated and non-silylated Co/SBA catalysts.

Table 2
The activity and selectivity of different catalysts for Fischer–Tropsch synthesis.

Catalyst	CO conversion (%)[a]	Hydrocarbon selectivity (wt%)					
		CH_4	C_{2-4}	C_{5+}	C_{5-11}	C_{12-18}	C_{19+}
Co/SBA	60.82	9.53	6.55	83.92	40.56	27.11	16.25
Co/S-SBA	77.15	11.76	9.06	79.18	36.24	26.75	16.20
S-Co/SBA	52.82	19.18	14.89	65.93	39.76	21.21	4.96

[a] Reaction conditions: $T=513$ K, $n(H_2)/n(CO)=2.0$, GHSV$=1000\ h^{-1}$ and $P=2.0$ MPa.

The silylation markedly influenced the reduction processes of Co/SBA catalysts. According to the literature [36], the first reduction step of Co_3O_4 ($Co_3O_4 \rightarrow CoO$) was fast (giving a sharp low-temperature peak), and the slow CoO reduction step resulted in a broad profile (see Fig. 5). It was believed that the broad second region was dependent on the interaction between CoO and the support. Both Co/SBA and S-Co/SBA showed a broad reduction peak in the second reduction step ($CoO \rightarrow Co^0$), indicating their strong interaction with support. The silylated catalysts S-Co/SBA had the lowest reducibility, which was ascribed to the steric hindrance of grafted $-Si(CH_3)_3$ towards the accessibility of the H_2 to cobalt oxides.

3.6. Performance of silylated Co catalysts

The performance of silylated Co catalysts for an FT synthesis is listed in Table 2 and they followed the activity order Co/S-SBA > Co/SBA > S-Co/SBA under the same conditions, which was in accordance with the order of their reducibility observed by TPR. Co/S-SBA catalyst had the highest CO conversion as the result of the silylation prior to the introduction of cobalt into the support, which weakened the cobalt-support interaction and then enhanced the reducibility of cobalt oxide species. Consequently, S-Co/SBA showed the lowest CO conversion compared with Co/SBA.

An enhanced formation of methane and light hydrocarbons (C_2–C_4) was observed and the selectivity for higher hydrocarbons (C_{19+}) significantly decreased with the addition of HMDS. Ojeda et al. [21] found that the CO conversion rate increased over the silylated catalyst and no changes were found for the chain-growth probability [21]. However, it should be noted that they did not detect any changes in cobalt reducibility after the silylation. In the present case, such a low activity and high C_1 selectivity could be related to the low reducibility of cobalt species on an S-Co/SBA. Besides, this might also be ascribed to either the reduction of the accessibility of the reactants to active sites by the presence of organic groups incorporated into Co/SBA catalyst, or the prevention of the re-adsorption of α-olefins and the chain growth by the steric hindrance of grafted $-Si(CH_3)_3$ [22]. As a result, the S-Co/SBA catalyst showed the low activity and high selectivity towards methane.

4. Conclusions

A series of silylated Co/SBA-15 catalysts were prepared by different post-grafting routes via vapor-phase silylation. It was found that their Co_3O_4 crystallite size and reducibility were influenced by silylation routes. Co/S-SBA catalyst showed the largest Co_3O_4 crystallite size and the highest reducibility, and then more active and low methane selectivity than S-Co/SBA in an FT synthesis. This proved that the silylation before the cobalt impregnation had a positive effect on both activity and selectivity in an FT synthesis.

Acknowledgment

This work was supported by the State Key Foundation Program for Development and Research of China (Contract no. 2005CB221402) and the Natural Science Foundation of China (Contract no. 21076218 and 21003149).

References

[1] M.B. D'Amore, S. Schwarz, Chem. Commun. (1999) 121.
[2] V.M. Gun'ko, V.V. Turov, V.M. Bogatyrev, B. Charmas, J. Skubiszewska-Zieba, R. Leboda, S.V. Pakhovchishin, V.I. Zarko, L.V. Petrus, O.V. Stebelska, M.D. Tsapko, Langmuir 19 (2003) 10816.
[3] I. Rodriguez, S. Iborra, A. Corma, F. Rey, J.L. Jordá, Chem. Commun. 7 (1999) 593.
[4] I.K. Mbaraka, D.R. Radu, V.S.-Y. Lin, B.H. Shanks, J. Catal. 219 (2003) 329.
[5] S. Dai, M.C. Burleigh, Y. Shin, C.C. Morrow, C.E. Barnes, Z. Xue, Angew. Chem. Int. Ed. 38 (1999) 1235.
[6] A.M. Liu, K. Hidajat, S. Kawi, D.Y. Zhao, Chem. Commun. 13 (2000) 1145.
[7] V.S.Y. Lin, C.Y. Lai, J.G. Huang, S.A. Song, S. Xu, J. Am. Chem. Soc. 123 (2001) 11510.
[8] W.Z. Zhou, J.M. Thomas, D.S. Shephard, B.F.G. Johnson, D. Ozkaya, T. Maschmeyer, R.G. Bell, Q.F. Ge, Science 280 (1998) 705.
[9] W. Zhang, X. Lu, J. Xiu, Z. Hua, L. Zhang, M. Robertson, J. Shi, D. Yan, J.D. Holmes, Adv. Funct. Mater. 14 (2004) 544.
[10] A.P. Wight, M.E. Davis, Chem. Rev. 102 (2002) 3589.
[11] A. Corma, J.L. Jordá, M.T. Navarro, F. Rey, Chem. Commun. 17 (1998) 1899.
[12] D. Brunel, A. Cauvel, F.D. Renzo, F. Fajula, B. Fubini, B. Onida, E. Garrone, New J. Chem. 24 (2000) 807.
[13] A.S. Maria Chong, X.S. Zhao, A.T. Kustedjo, S.Z. Qiao, Microporous Mesoporous Mater. 72 (2004) 33.
[14] G. Jacobs, T.K. Das, Y.Q. Zhang, J.L. Li, G. Racoillet, B.H. Davis, Appl. Catal. A: Gen. 233 (2002) 263.
[15] M.E. Dry, Catal. Today 6 (1990) 183.
[16] E. Iglesia, S.L. Soled, R.A. Fiato, J. Catal. 137 (1992) 212.
[17] B.G. Johnson, C.H. Bartholomew, D.W. Goodman, J. Catal. 128 (1991) 231.
[18] M.D. Skowronska-Ptasinska, M.L.W. Vorstenbosch, R.A. van Santen, H.C.L. Abbenhuis, Angew. Chem. Int. Ed. 41 (2002) 637.
[19] J.M. Fraile, J.I. García, J.A. Mayoral, E. Vispe, Appl. Catal. A: Gen. 245 (2003) 363.
[20] D.J. Kim, B.C. Dunn, P. Cole, G. Turpin, R.D. Ernst, R.J. Pugmire, M. Kang, J.M. Kim, E.M. Eyring, Chem. Commun. (2005) 1462.
[21] M. Ojeda, F.J. Prez-Alonso, P. Terreros, S. Rojas, T. Herranz, M.L. Granados, J.L.G. Fierro, Langmuir 22 (2006) 3131.
[22] L. Shi, J. Chen, K. Fang, Y. Sun, Fuel 87 (2008) 521.
[23] S. Shen, F. Chen, P.S. Chow, P. Phanapavudhikul, K. Zhu, R.B.H. Tan, Microporous Mesoporous Mater. 92 (2006) 300.
[24] C.T. Kirk, Phys. Rev. B 38 (1988) 1255.
[25] L. Bois, A. Bonhommé, A. Ribes, B. Pais, G. Raffin, F. Tessier, Colloids Surf. A: Physicochem. Eng. Aspects 221 (2003) 221.

[26] J. Chen, Q. Li, R. Xu, F. Xiao, Angew. Chem., Int. Ed. 34 (1995) 2694.
[27] D. Lin-Vien, N.B. Colthup, W.G. Fateley, J.G. Grasselli, Infrared and Raman Characteristic Frequencies of Organic Molecules, Academic Press, 1991.
[28] L.D. White, C.P. Tripp, J. Colloid Interface Sci. 224 (2000) 417.
[29] X. Lin, G.K. Chuah, S. Jaenicke, J. Mol. Catal. A: Chem. 150 (1999) 287.
[30] S. Zheng, L. Gao, J. Guo, Mater. Chem. Phys. 71 (2001) 174.
[31] B. Ernst, S. Libs, P. Chaumette, A. Kiennemann, Appl. Catal. A: Gen. 186 (1999) 145.
[32] P. Arnoldy, J.A. Moulijn, J. Catal. 93 (1985) 38.
[33] B.D. Cullity, Elements of X-ray Diffraction, Addision-Wesley, London, 1978.
[34] Y. Zhang, M. Shinoda, N. Tsubaki, Catal. Today 93 (2004) 55.
[35] B. Sexton, A. Hughes, T. Turney, J. Catal. 97 (1986) 390.
[36] H.F. Xiong, Y.H. Zhang, K. Liew, J.L. Li, J. Mol. Catal. A: Chem. 295 (2008) 68.